Soft Matter

PAPER

Check for updates

Cite this: *Soft Matter*, 2019, **15**, 7018

Sound attenuation in stable glasses

Lijin Wang, [ab] Ludovic Berthier, [c] Elijah Flenner, *[b] Pengfei Guan*[a] and Grzegorz Szamel [b]

Received 30th May 2019,
Accepted 2nd August 2019

DOI: 10.1039/c9sm01092k

rsc.li/soft-matter-journal

Understanding the difference between the universal low-temperature properties of amorphous and crystalline solids requires an explanation for the stronger damping of long-wavelength phonons in amorphous solids. A longstanding sound attenuation scenario, resulting from a combination of experiments, theories, and simulations, leads to a quartic scaling of sound attenuation with the wavevector, which is commonly attributed to the Rayleigh scattering of sound. Modern computer simulations offer conflicting conclusions regarding the validity of this picture. We simulate glasses with an unprecedentedly broad range of stabilities to perform the first microscopic analysis of sound damping in model glass formers across a range of experimentally relevant preparation protocols. We present convincing evidence that quartic scaling is recovered for small wavevectors irrespective of the glass's stability. With increasing stability, the wavevector where the quartic scaling begins increases by approximately a factor of three and the sound attenuation decreases by over an order of magnitude. Our results uncover an intimate connection between glass stability and sound damping.

1 Introduction

Many theoretical descriptions of sound attenuation in low temperature (athermal) amorphous solids predict a quartic scaling of sound attenuation with the wavevector. Early arguments, used to explain the plateau in the temperature dependence of thermal conductivity,[1,2] invoked the picture of the scattering of sound waves by uncorrelated inhomogeneities that are much smaller than the wavelengths, which is the physical scenario known as Rayleigh scattering. In several theories, these inhomogeneities have been modeled as local fluctuations of elastic constants.[3–8] These theories predict that the sound attenuation scales with the fourth power of the wavevector, $\Gamma_\lambda(k) \sim k^4$ (λ = L denotes longitudinal waves and λ = T denotes transverse waves) for small wavevector k. Mean-field theories[9–12] arrive at the same prediction, albeit in a different way. Yet another theoretical treatment, the soft-potential model, predicts that a quartic scaling regime exists due to phonons interacting with soft modes.[13]

Longitudinal sound attenuation can be directly obtained from X-ray and light scattering experiments. A compilation of many experimental results[14–28] shows that the wavevector dependence of the longitudinal sound attenuation parameter, $\Gamma_L(k)$, can be divided into three regimes: (1) $\Gamma_L(k) \sim k^2$ for low k; (2) $\Gamma_L(k) \sim k^4$ for an intermediate k regime; and (3) $\Gamma_L(k) \sim k^2$ for large k. While the intermediate wavevector quartic and the large wavevector quadratic scalings of the sound attenuation parameter are well-documented, the small wavevector quadratic dependence was only seen in a few experiments.[17–20] Because the experiments are performed at finite temperature and the small wavevector quadratic scaling increases with temperature, the small wavevector quadratic scaling can be ascribed to thermal and anharmonic effects.[5]

Computer simulations offer a conflicting view of these results. Most computer studies investigate sound attenuation in the limit of zero temperature in order to remove anharmonic effects. To our knowledge, no simulation reproduced the $\Gamma_L(k) \sim k^2$ scaling observed at small wavevectors in experiments,[17–20] including a recent finite temperature study of Mizuno and Mossa[29] that included anharmonic effects. Regarding the quartic Rayleigh scattering regime, no firm conclusion can be drawn either. By simulating large glasses created by quenching configurations from a mildly supercooled liquid, Gelin *et al.*[30] found a logarithmic correction to the quartic scaling, $\Gamma_\lambda(k) \sim k^4 \ln(k)$. They invoked the existence of correlated inhomogeneities of the elastic constants[31] to rationalize this observation. However, a more recent, larger-scale study[32] of harmonic spheres close to their unjamming transition confirmed the Rayleigh scattering scenario in 2D glasses and conjectured its validity in 3D glasses. Finally, a very recent preprint[33] (which appeared when the present paper was being finalized for submission) presented the first convincing evidence of the small wavevector quartic scaling of the transverse sound attenuation in a 3D glass created by

[a] *Beijing Computational Science Research Center, Beijing 100193, P. R. China. E-mail: pguan@csrc.ac.cn*
[b] *Department of Chemistry, Colorado State University, Fort Collins, Colorado 80523, USA. E-mail: flennere@gmail.com*
[c] *Laboratoire Charles Coulomb (L2C), University of Montpellier, CNRS, 34095 Montpellier, France*

This journal is © The Royal Society of Chemistry 2019

quenching from a mildly supercooled liquid. However, the status of the longitudinal sound attenuation, even for simple glass-formers in the zero-temperature harmonic limit, remains unsettled.

To our knowledge, all prior simulations investigated sound attenuation in glasses with stabilities dramatically different from those of typical laboratory glasses, preventing direct comparison between results obtained for simulated and real materials. This constraint is imposed by the large preparation times required to equilibrate systems close to the experimental glass transition, which, therefore, cannot be simulated using conventional techniques. In this work, we use an efficient swap Monte-Carlo algorithm[34] that was recently developed[35,36] to prepare glasses with stabilities comparable to, or even exceeding, the stability of experimental glasses. If we quantify the glass stability in terms of cooling rate, the improvement due to the swap algorithm is equivalent to decreasing the cooling rate by more than 10 orders of magnitude, thus closing the gap between previous computer investigations and realistic materials. In previous studies, it has been demonstrated that both the low-frequency vibrational properties[37] and mechanical properties[38] of computer generated glasses dramatically evolve upon increasing the glass stability over such a broad range.

We find that changing the glass stability over a broad range fully clarifies the elusive picture of sound attenuation. Generally, sound attenuation decreases with increasing stability, implying that more stable glasses are also less dissipative solids (classical zero temperature crystalline solids are non-dissipative). More importantly, we find the wavevector dependence of sound attenuation at low wavevectors exhibits a quartic scaling, for both transverse and longitudinal modes and in glasses with very different stabilities. Thus, we unambiguously demonstrate the universality of the Rayleigh scattering scaling in 3D glasses. The quartic scaling of the sound attenuation with the wavevector is more prominent in more stable glasses, which adds to the conjectured connection between glass stability and sound damping.

2 Methods

2.1 Simulation details

We perform computer simulations using a three-dimensional cubic system composed of polydisperse particles with equal mass $m = 1$. The distribution of particle diameters σ follows $P(\sigma) = \frac{A}{\sigma^3}$, where $\sigma \in [0.73, 1.63]$ and A is a normalization factor. The cross-diameter σ_{ij} is determined according to a non-additive mixing rule, $\sigma_{ij} = \frac{\sigma_i + \sigma_j}{2}(1 - \varepsilon|\sigma_i - \sigma_j|)$ with $\varepsilon = 0.2$. The interaction between two particles i and j is provided by the inverse power law potential, $V(r_{ij}) = \left(\frac{\sigma_{ij}}{r_{ij}}\right)^{12} + V_{\mathrm{cut}}(r_{ij})$, when the separation r_{ij} is smaller than the potential cutoff $r_{ij}^c = 1.25\sigma_{ij}$, and zero otherwise. Here, $V_{\mathrm{cut}}(r_{ij}) = c_0 + c_2\left(\frac{r_{ij}}{\sigma_{ij}}\right)^2 + c_4\left(\frac{r_{ij}}{\sigma_{ij}}\right)^4$, and the coefficients c_0, c_2 and c_4 are set to guarantee the continuity of $V(r_{ij})$ at r_{ij}^c up to the second derivative.

We produce zero-temperature glasses by instantaneously quenching supercooled liquids equilibrated through the swap Monte Carlo algorithm at different parent temperatures T_p, which controls the glass's stability,[37,38] to their local potential minima using the fast inertial relaxation engine minimization.[39] We calculate the normal modes by diagonalizing the dynamic matrix using Intel Math Kernel Library (https://software.intel.com/en-us/mkl/) and ARPACK (http://www.caam.rice.edu/software/ARPACK/). We study glasses with T_p ranging from well above the onset of supercooling, denoted as $T_p = \infty$, down to $T_p = 0.062$, which is about 60% of the mode-coupling temperature $T_c \approx 0.108$.[36] The onset of slow dynamics in an equilibrated fluid occurs around $T_o = 0.2$. The parent temperature $T_p = 0.062$ is lower than the estimated experimental glass temperature $T_g \approx 0.072$ for this model,[36] and thus the glass with $T_p < 0.072$ qualifies as ultrastable. One robust measure of stability is the energy at the potential energy minimum,[40–43] the inherent structure energy E_{IS}. Shown in Fig. 1 is the inherent structure energy for our glasses as a function of parent temperature T_p, and we find that the inherent structure energy dramatically drops below the onset temperature T_o. The particle number N varies between 48 000 and 1 000 000 for glasses at $T_p = \infty$, and between 48 000 and 192 000 for glasses with $0.062 \leq T_p \leq 0.120$. For all glasses studied the number density $\rho = 1.0$.

2.2 Sound attenuation

We use two different methods to obtain sound attenuation: (1) we calculate the $T = 0$ dynamic structure factor utilizing the eigenvalues and eigenvectors of the dynamic matrix;[44] and (2) we study the decay of an excited sound wave in the harmonic approximation.[30]

We calculate the $T = 0$ dynamic structure factors using the eigenvalues and eigenvectors of the dynamic matrix,[44]

$$S_\lambda(k,\omega) = \left(\frac{k^2}{N\omega^2}\right)\sum_{n=1}^{3N-3} F_{n,\lambda}(k)\delta(\omega - \omega_n), \qquad (1)$$

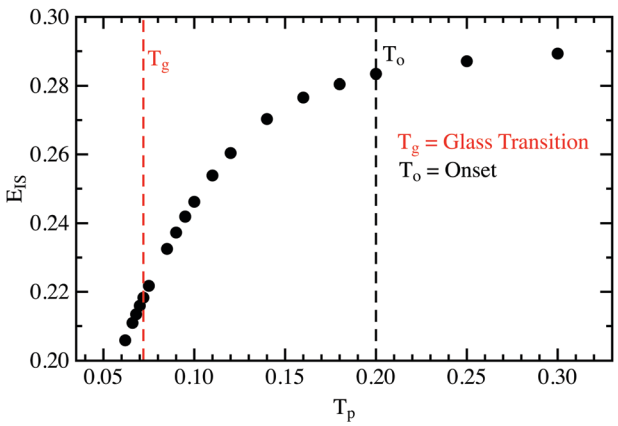

Fig. 1 The inherent structure energy *versus* the parent temperature. The onset of slow dynamics T_o and the estimated glass transition temperature T_g[36] are shown. The glass becomes more stable with decreasing inherent structure energy.

where λ is T for transverse or L for the longitudinal structure factor, ω_n is the frequency (square root of the eigenvalue) associated with the n-th eigenvector. The sum is taken over all but the three modes correspond to a universal translation. In eqn (1)

$$F_{n,\mathrm{T}}(k) = \left|\sum_{j=1}^{N}(\mathbf{e}_{n,j}\times\hat{\mathbf{k}})e^{i\mathbf{k}\cdot\mathbf{r}_j^0}\right|^2, \quad (2)$$

and

$$F_{n,\mathrm{L}}(k) = \left|\sum_{j=1}^{N}(\mathbf{e}_{n,j}\cdot\hat{\mathbf{k}})e^{i\mathbf{k}\cdot\mathbf{r}_j^0}\right|^2, \quad (3)$$

where $\mathbf{e}_{n,j}$ is the polarization vector of particle j in the n-th eigenvector, $\mathbf{r}_j^0$ is the position of particle j in the inherent structure, and $\mathbf{k}$ is the wavevector satisfying periodic boundary conditions, $k \equiv |\mathbf{k}|$ and $\hat{\mathbf{k}} = \mathbf{k}/|\mathbf{k}|$. We extract the damping coefficients Γ_λ and the characteristic frequencies Ω_λ by fitting $S_\lambda(k,\omega)$ to a damped harmonic oscillator model,[45]

$$S_\lambda(k,\omega) \propto \frac{\Omega_\lambda^2(k)\Gamma_\lambda(k)}{[\omega^2-\Omega_\lambda^2(k)]^2+\omega^2\Gamma_\lambda^2(k)}. \quad (4)$$

Another method to determine Γ_λ and Ω_λ is to study the decay of excited sound waves in the harmonic approximation, and most of our results shown in this work are from this method (unless specified). Specifically, following ref. 30, we excite a sound wave at $t = 0$ by giving each particle a velocity $\dot{\mathbf{u}}_i^0 = \mathbf{a}_\lambda \sin(\mathbf{k}\cdot\mathbf{r}_i^0)$, where $\mathbf{a}_\mathrm{L} \propto \hat{\mathbf{k}}$ and $\mathbf{a}_\mathrm{T}\cdot\mathbf{k} = 0$. We then numerically solve the equations of motion,

$$\ddot{\mathbf{u}}_i(t) = -\sum_{j=1}^{N}\mathbf{D}_{ij}\cdot\mathbf{u}_j(t) + \dot{\mathbf{u}}_i^0\delta(t). \quad (5)$$

Here, D_{ij} is the dynamic matrix and $\mathbf{u}_i(t)$ denotes the displacement of particle i at t from its inherent structure position. We calculate the velocity correlation function,

$$C_\lambda(t) = \frac{\sum_{i=1}^{N}\dot{\mathbf{u}}_i(0)\cdot\dot{\mathbf{u}}_i(t)}{\sum_{i=1}^{N}\dot{\mathbf{u}}_i(0)\cdot\dot{\mathbf{u}}_i(0)}, \quad (6)$$

and fit it to

$$C_\lambda(t) = \exp(-\Gamma_\lambda(k)t/2)\cos(\Omega_\lambda(k)t), \quad (7)$$

to determine the frequency Ω_λ and the sound attenuation Γ_λ. Since the calculation affords Ω_λ through a fit for a fixed $\mathbf{k}$, the wavevector is precisely known but there is uncertainty in Ω_λ.

Shown in Fig. 2 is an example of the excited sound wave method.[30] The snapshots in Fig. 2 show the velocity field for $\mathbf{k} = (0, 4\pi/\mathrm{L}, 0)$ in a 48 000 particle system for times at the peak values of $C_\mathrm{T}(t)$ indicated in the figure. As expected, the sound wave is scattered and the initial velocity profile decays.

The two methods introduced above encode the same dynamical information, but there exists a finite size effect that is impossible to correct by using the normal mode analysis. See the Appendix section for details on how we account for this finite size effect and for details on how we obtain Γ_λ.

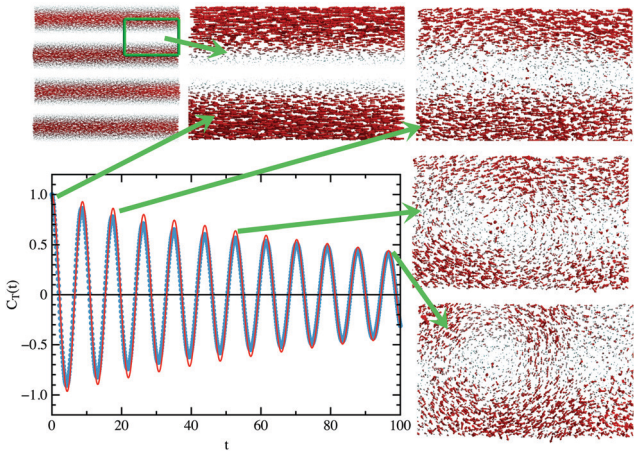

Fig. 2 Decay of $C_\mathrm{T}(t)$ for a transverse excitation with a wavevector $\mathbf{k} = (0, 4\pi/\mathrm{L}, 0)$ for our most stable glass, $T_\mathrm{p} = 0.062$ (blue circles). The red curve is a fit to $C_\mathrm{T}(t) = \exp(-\Gamma_\lambda t/2)\cos(\Omega_\lambda t)$. The velocity field for the whole system is shown in the upper left corner and a section at representative times corresponding to the peaks in $C_\mathrm{T}(t)$ is indicated by the arrows. The longer and brighter red arrows indicate larger velocities.

3 Sound attenuation in stable glasses

Shown in Fig. 3 are $\Gamma_\lambda(k)$ for a range of stabilities for (a) transverse sound waves and (b) longitudinal sound waves. For large wavevectors we observe quadratic scaling, which is consistent with previous results. There is no difference in the attenuation for $T_\mathrm{p} = 0.2$ and $T_\mathrm{p} = \infty$ suggesting that zero-temperature glasses quenched from parent temperatures above the onset temperature $T_\mathrm{o} = 0.2$ have identical attenuation. There is a crossover to quartic scaling, Rayleigh scaling, for our least stable glasses $T_\mathrm{p} = \infty$ and our most stable glasses $T_\mathrm{p} = 0.062$. Therefore, $\Gamma_\lambda(k) = B_\lambda k^4$ for small wavevectors irrespective of the glass's stability.

To examine the stability dependence of B_λ and the possibility of a logarithmic correction, in Fig. 3 we plot $\Gamma_\lambda(k)/k^4$ for $T_\mathrm{p} = \infty$, 0.1, 0.085, 0.075, and 0.062 for transverse sound (c) and the longitudinal sound (d). There is a factor of 15 decrease in B_λ from our least stable glass to the most stable glass. We note that in the representation in Fig. 3 a straight line with a negative slope would indicate the $-k^4\ln(k)$ scaling suggested by Gelin *et al.*[30] We can identify a range of wavevectors that is described by $\Gamma_\mathrm{T}(k) \sim -k^4\ln(k)$ for our least stable glasses, but this fit appears to be just a crossover from quadratic scaling at large wavevectors to quartic scaling at small wavevectors. Indeed, we observe a distinct plateau at low wavevectors, indicating a purely quartic scaling without a logarithmic correction. The small wavevector quartic scaling is clearly observed for the least stable glass $T_\mathrm{p} = \infty$ and the most stable glass $T_\mathrm{p} = 0.062$, and thus it would be expected to exist for intermediate stability.

As noted by Monaco and Mossa[45] when studying glasses created by quenching from mildly supercooled liquids, the transverse and longitudinal sound attenuation differ by a constant factor when examined as a function of frequency $\omega = v_\lambda k$, where

This journal is © The Royal Society of Chemistry 2019

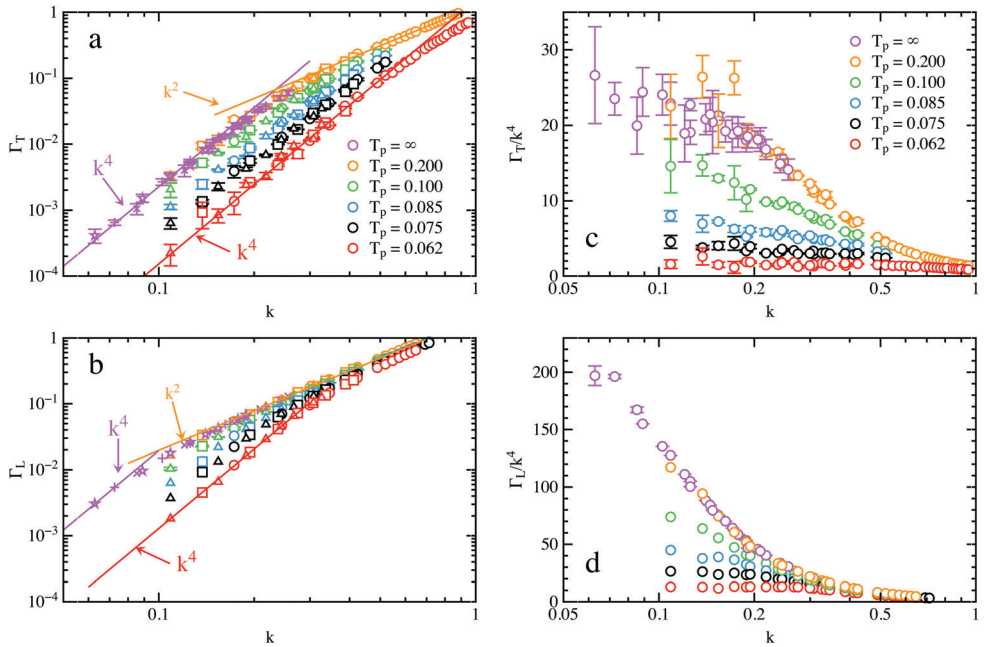

Fig. 3 Wavevector k dependence of sound attenuation (a) $\Gamma_T(k)$ and (b) $\Gamma_L(k)$ in poorly annealed glasses ($T_p = \infty$) to stable glasses ($T_p = 0.062$). The different symbols denote different system sizes: star = 1000 K, plus = 600 K, × = 450 K, triangle = 192 K, square = 96 K, and circle = 48 K. The k^2 dependence is evident at large wavevectors and the crossover to k^4 scaling can be seen for $T_p = \infty$ and $T_p = 0.062$. The reduced sound attenuation (c) Γ_T/k^4 and (d) Γ_L/k^4. A straight line with a negative slope would indicate a logarithmic correction, which is valid only for a small range of wavevectors.

$v_T = \sqrt{G/\rho}$, $v_L = \sqrt{(K + 4G/3)/\rho}$, G is the shear modulus, and K is the bulk modulus, Fig. 4. We find $\Gamma_L(\omega) = \Gamma_T(\omega)/n$ irrespective of the glass's stability, but the scaling factor n is stability dependent with $n \approx 5$ for our poorly annealed glass, $T_p = \infty$, and $n \approx 3$ for our most stable glass, $T_p = 0.062$, indicating a decreasing difference between $\Gamma_T(\omega)$ and $\Gamma_L(\omega)$ with increasing stability. This scaling suggests that the sound attenuation is governed by a stability dependent frequency (time) scale and possibly not a characteristic length scale. However, a changing length scale cannot be ruled out.

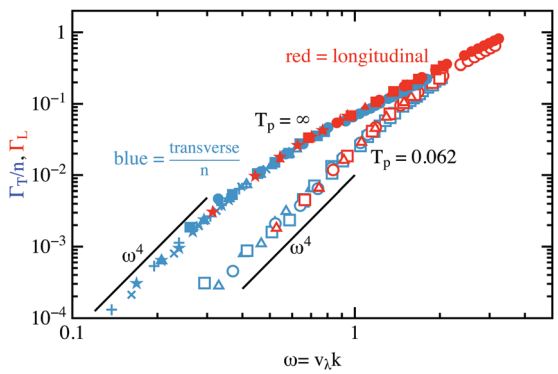

Fig. 4 Frequency $\omega = v_\lambda k$ dependence of sound attenuation in our least stable glass $T_p = \infty$ (filled symbols) and our most stable glass $T_p = 0.062$ (open symbols). The different symbols denote different system sizes: star = 1000 K, plus = 600 K, × = 450 K, triangle = 192 K, square = 96 K, and circle = 48 K. The red symbols are the results of the longitudinal attenuation and the blue symbols are results of the transverse attenuation. The transverse attenuation is scaled by a T_p dependent factor n, where $n = 5$ for $T_p = \infty$ and $n = 3$ for $T_p = 0.062$.

With increasing stability, the glass becomes less dissipative and quartic scalings of Γ_T and Γ_L start at larger wavevectors. The wavevector at which the quartic scaling begins depends on the polarization, transverse or longitudinal, of the sound wave. In contrast, if we plot the sound attenuation as a function of frequency, the frequency where the quartic scaling begins does not depend on the transverse or longitudinal sound wave. Again, this crossover frequency increases with increasing stability The glass becomes more uniform, resulting in a decrease in the dissipation[30,31] with an increase in the stability.

For small and intermediate wavevectors the wavevector-dependent speed of sound $v_T(k) = \Omega_T/k$ is a well defined quantity. In particular, for every parent temperature the $k \to 0$ limit is given by $\sqrt{G/\rho}$, which is shown as horizontal lines in Fig. 5. However, with increasing wavevector different methods lead to slightly but systematically different results for the wavevector-dependent speed of sound. If we determine the speed of sound from the fit to the frequency-dependent dynamic structure factor (filled circles), the resulting quantity exhibits a minimum, which has been reported in previous simulations[8,30,32,45] and experiments.[23,24,47] This minimum is replaced by a plateau for our stable glasses. However, if we rely upon the fit to the time-dependent function $C_\lambda(t)$ (open symbols), the wavevector-dependent speed of sound exhibits a more pronounced minimum, which is also present for the stable glasses. The difference between the two methods is small (less than 7% for wavevectors shown in Fig. 5) but systematic.

It is expected that the two methods could disagree when the excitation is no longer well described as a propagating sound wave, which is generally associated when the mean free path is

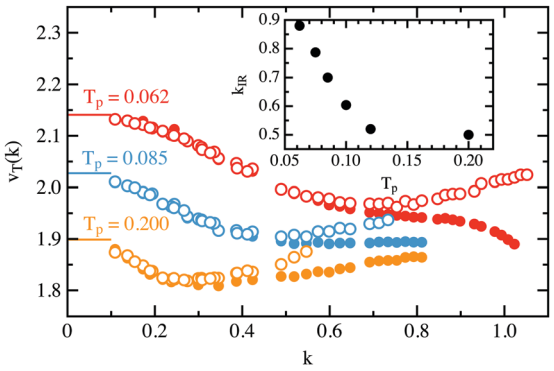

Fig. 5 The wavevector dependence of sound speed for different parent temperatures T_p. The horizontal lines indicate the corresponding macroscopic values in the long-wavelength limit. The open symbols are obtained through fits to $C_T(t)$ and the closed symbols are obtained through fits to $S_T(k;\omega)$. (inset) Ioffe-Regel wavevector k_{IR} as a function of T_p.

equal to half the wavelength, *i.e.* the Ioffe-Regel limit. Shown in the inset in Fig. 5 is the Ioffe-Regel limit obtained from when $\Omega_T(k_{IR}) = \pi\Gamma_T(k_{IR})$ as a function of the parent temperature. For this calculation we used Ω_T determined from the fits to the dynamic structure factor. The result is not sensitive to which method is used to determine Ω_T. For $T_p = 0.2$, $k_{IR} \approx 0.5$ and for $T_p = 0.062$, $k_{IR} \approx 0.87$. Both of these quantities lie slightly above where the two methods to obtain the wavevector-dependent speed of sound begin to diverge. Thus, the classification of these excitations as propagating sound waves is breaking down for wavevectors slightly smaller than k_{IR}.

Nevertheless, we find that increasing the stability of the glass allows propagating sound waves at smaller wavelengths, and this can be quantified by the change in k_{IR}. For decreasing T_p, k_{IR} increases by a factor of 1.8 over our range of stabilities. For wavevectors above k_{IR} it is expected that the vibrations are more localized and there is a change in the energy transport from a propagating regime below k_{IR} to a diffusive regime above k_{IR}.[48–50] Therefore, the decreased dissipation and the increase in k_{IR} should have significant effects on the thermal conductivity and the stability dependence of thermal energy transport.

4 Connection between sound attenuation, vibrational modes, and the boson peak

A recurring idea is that sound attenuation and the excess in vibrational modes over the Debye theory are intimately connected. Recall that in the Debye theory the density of states increases with a decrease in the speed of sound. Using this idea, the minimum in $v_T(\omega)$ has been associated with an increase of the density of states $D(\omega)$ and the boson peak using a generalized plane wave approach.[45] However, we find that the description of the vibrational modes as well defined sound waves breaks down for wavevectors below the boson peak whose position is close to k_{IR}.[51]

In previous studies[37,52] it was found that the low-frequency modes could be divided into extended and quasi-localized modes. The density of the low-frequency extended modes obeys the Debye theory and the density of the localized modes $D_{loc} = A_4\omega^4$. Therefore, these localized modes are the modes in excess of the Debye theory. The density of the low-frequency quasi-localized modes was found to decrease significantly with the glass stability.[37] Here we find that the sound attenuation and the Rayleigh scattering plateau Γ_λ/k^4 also decrease the glass stability rapidly. In Fig. 6 we show that coefficient A_4 quantifying the density of the low-frequency quasi-localized modes and the Rayleigh scattering plateau $B_T = \Gamma_T/k^4$ are proportional to each other, $B_T \propto A_4$.

Our findings for the transverse sound attenuation in moderate and low stability glasses are in general agreement with the very recent results of Moriel *et al.*[33] Specifically, both our study and that by Moriel *et al.* find quartic small wavevector scaling of the transverse sound attenuation in 3D glasses. Moriel *et al.* also investigated the dependence of the sound attenuation of glasses with different densities of low-frequency quasi-localized modes. They found that the decreasing density of these modes correlates with the decreasing extent of the intermediate regime between the small wavevector quartic scaling and the large wavevector quadratic scaling, which can be fitted to the $-k^4 \ln k$ form proposed by Gelin *et al.*[30] Our finding $B_T \propto A_4$ significantly extends the qualitative correlation found by Moriel *et al.*[33]

A generalized Debye model of Mizuno and Ikeda[32] and the theoretical study of Schirmacher *et al.*,[4] referred to as the heterogeneous elasticity theory, both relate the excess number of low-frequency modes above the Debye model, $D_{ex}(\omega)$, to sound attenuation. Both of these treatments predict that $D_{ex} \approx 4B_T/(\pi k_D{}^2 v_T{}^6)\omega^4$, where $k_D = (6\pi\rho)^{1/3}$, for small wavevectors. Physically, these are the same modes as identified in ref. 37 and 52 and thus $D_{ex}(\omega)/\omega^4 = 4B_T/(\pi k_D{}^2 v_T{}^6)$ can be identified with A_4. We find that A_4 is 20% larger than $4B_T/(\pi k_D{}^2 v_T{}^6)$ for our poorly annealed glass and 150% larger for our most stable glass. Mizuno and Mossa[29] compare the heterogeneous elasticity theory to zero temperature and finite temperature simulations and find that the theory captures the main features of the

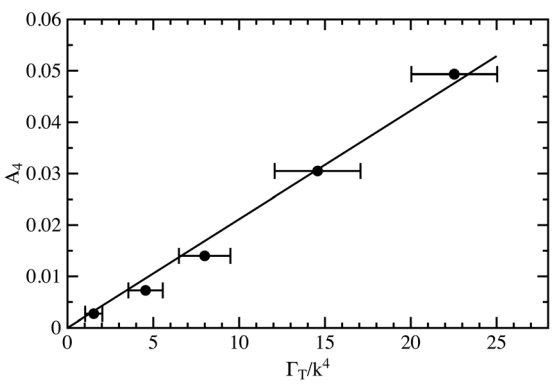

Fig. 6 The coefficient A_4 describing the density of low-frequency quasi-localized modes, $D_{loc} = A_4\omega^4$ correlates very well with the plateau height of Γ_T/k^4 for small wavevectors. They are both strongly suppressed when glass stability increases.

This journal is © The Royal Society of Chemistry 2019

frequency dependence of the transverse sound attenuation and velocity, but there were quantitative differences. Therefore, the models[4,32] are currently not quantitatively predictive and get worse with increasing stability.

A recent experiment by Pogna *et al.*[46] reported on a connection between sound attenuation and the boson peak. They find a decrease in the boson peak height and sound attenuation for hyperaged amber (conjectured to be much more stable) compared to annealed amber (with ordinary stability), which mirrors our results.[37] Pogna *et al.* used the fluctuating elasticity theory of Schirmacher *et al.*[5] (which predicts the quartic scaling of sound attenuation with the wavevector) to fit the vibrational density of states. There are two main parameters in the theory, one quantifies the strength of the disorder and is related to the width of the local elastic constant distribution, and another quantifying the spatial range of correlations of elasticity. They concluded that upon lowering the fictive temperature by 9% there was a six percent decrease of the strength of the fluctuations and a 22% increase of the elastic correlation length. Therefore, they conjectured that the change of the low-frequency vibrational properties is mainly driven by an increased elastic correlation length. Future work should examine the change of the disorder strength and the elastic correlation length with stability more directly to verify this conclusion.

A competing theoretical explanation for the relationship between sound attenuation and the boson peak is that the sound modes interact with additional soft modes,[13] the soft potential model. Examination and evaluation of the soft potential model requires the determination of several parameters, and this exercise is left for future work.

5 Discussion

The idea that a Rayleigh scattering mechanism may be responsible for the small wavevector scaling of sound attenuation spans for over 60 years.[32,53] Mizuno and Ikeda considered scattering of an elastic wave. Their analysis determined that $\Gamma_\lambda = \delta\gamma_\lambda{}^2 D_\lambda{}^3 \Omega_\lambda{}^4/(4\pi v_\lambda{}^3)$, where $\delta\gamma$ is the strength of the elastic inhomogeneities and D is their characteristic size.[32] Since it has been suggested that $k_{BP} = \omega_{BP}/v_T$ is related to the inverse of the length scale of elastic inhomogeneities,[3,47] and thus D, we checked to see if this was consistent with the quartic scaling regimes for Γ_T. We used the approach studied by Mizuno, Mossa, and Barrat[54] to obtain the strength $\delta\gamma_T = \delta G/G$, where δG is the fluctuations of the shear modulus, of the elastic inhomogeneities. We find that this naive approach does not correctly predict the change in the sound attenuation for each parent temperature. One unchecked assumption is that k_{BP} is related to the length scale of elastic inhomogeneities, and future work is needed to examine the spatial correlations of the elastic modulus and the relationship to k_{BP} and sound attenuation.

Recent experiments on amber aged for 110 million years suggest that the vibrational properties of amorphous materials are controlled by the distribution of elastic constants and their spatial correlation.[46] Future numerical studies should examine this relationship for simulated ordinary and stable glasses. The stability dependence of sound attenuation using ultrastable glasses, experimentally available *via* the method of physical vapor deposition,[55] has shown that sound damping decreases with increasing stability.[56] It would be interesting to examine the wavevector dependence of sound damping at low temperatures, where anharmonicities may come into play, for these ultrastable glasses. Mizuno and Mossa[29,57] found that anharmonicities change the small frequency sound attenuation from $\Gamma \sim \omega^4 \sim k^4$ to $\Gamma \sim \omega^{3/2} \sim k^{3/2}$, and the nature of this effect may be illuminated by its stability dependence.

Conflicts of interest

There are no conflicts to declare.

Appendix

Molecular dynamics simulations can be subject to effects due to the small size of the simulation cell compared to experimental systems and the use of periodic boundary conditions. Bouchbinder and Lerner recently commented on finite size effects in the calculation of the frequency width of phonon bands,[58] which indicates that finite size effects exist for the calculation of sound attenuation in amorphous solids. We find that there are strong finite size effects for the lowest wavevector sound waves in our simulations, especially for our most stable glasses. Here we describe a method to calculate sound attenuation that is independent of the system size.

One route to calculate the attenuation of sound waves is to study the decay of an excitation in the harmonic approximation as described in the Methods section. After exciting a sound wave, we study the decay of the velocity correlation function $C(t)$, eqn (6). For small wavevectors we expect that $C(t) = \exp(-\Gamma_\lambda t/2)\cos(\Omega_\lambda t)$.

To demonstrate that a finite size effect exists we can examine $C(t)$ for similar wavevectors in two systems of different sizes. The magnitude of the third smallest allowed the wavevector for the 96 K system $k_3^{96K} = 0.238$ and the magnitude of the second smallest allowed the wavevector $k_2^{48K} = 0.245$. The attenuation of these sound waves should be similar, but we find that they are very different, Fig. 7. Specifically, at long times the peak heights of the 96 K system are much larger than those of the 48 K system. However, $C(t)$ nearly overlaps at short times for both system sizes. To study the decay of $C(t)$ we calculate the envelope of $C(t)$, which is the absolute value of the maximum and minimum of the oscillations.

Shown in Fig. 8 on a linear-log scale is the envelope for three different sizes for a wavevector of similar magnitude. We note that the initial decay of all three envelopes is exponential, but there are deviations from the exponential decay at a system size dependent time. To determine Γ_λ we fit the envelope to $\exp(-\Gamma_\lambda t/2)$ up to a time when the decay is no longer exponential. Our uncertainty in Γ_λ reflects the uncertainty in this fitting range.

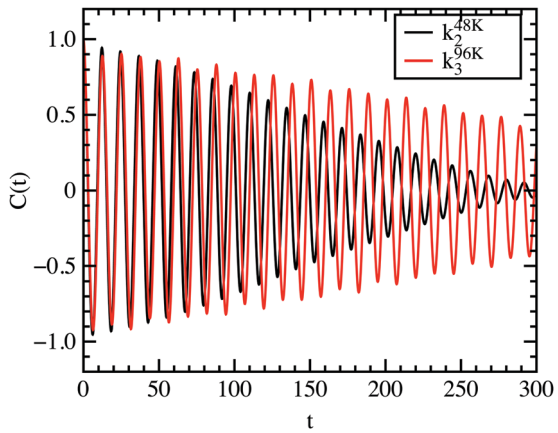

Fig. 7 Velocity correlation function $C(t)$ for wavevectors of similar magnitude, $k \approx 0.24$, for two different system sizes. The decay rate is clearly different and does not appear exponential.

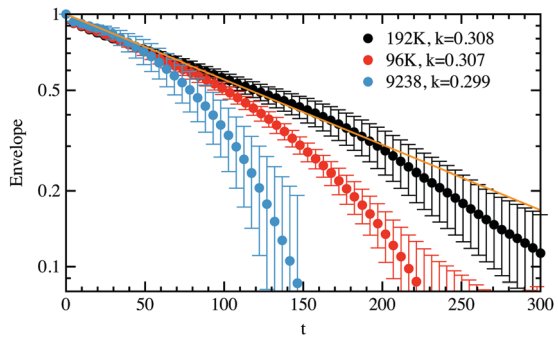

Fig. 8 The envelope of $C(t)$ for three system sizes for three wavevectors of nearly equal magnitude. The solid line represents a fit of the envelope to $\exp(-\Gamma_\lambda t/2)$.

Another method to obtain sound attenuation is through the dynamic structure factor $S_\lambda(k,\omega)$ using the eigenvalues and eigenvectors of the dynamic matrix, as described in the Methods section, or Fourier transforming $C(t)$. Sound attenuation Γ_λ is then obtained by fitting with the damped harmonic oscillator model, eqn (4).

Shown in Fig. 9 as red symbols are the results of fitting $S_T(k,\omega)$ and as blue symbols are the results of the restricted envelope fits. The different symbols indicate different system sizes. The inset shows an expanded view of a region of very similar wavevectors for four different system sizes. There is a clear finite size effect when Γ_T is found through fits of $S_T(k,\omega)$, which is removed by using the envelope fits.

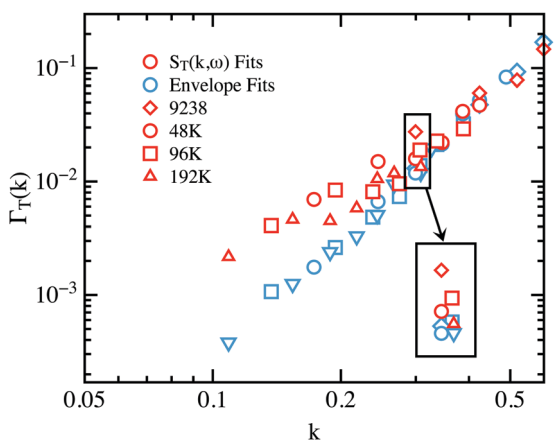

Fig. 9 Sound attenuation $\Gamma_T(k)$ calculated using fits to $S_T(k,\omega)$ (red) and the envelope fits (blue). The different symbols correspond to different system sizes. The inset shows an expanded view of the results for one wavevector. There is a clear finite size effect when $\Gamma_T(k)$ is obtained by fitting $S_T(k,\omega)$, which can be removed by using the restricted envelope fits.

Acknowledgements

We thank E. Lerner and E. Bouchbinder for correspondence on an earlier version of this work. L. W., E. F., and G. S. acknowledge funding from NSF DMR-1608086. This work was also supported by a grant from the Simons foundation (No. 454933 L. B.). L. W., and P. G. acknowledge support from the National Natural Science Foundation of China (No. 51571011), the MOST 973 Program (No. 2015CB856800), and the NSAF joint program (No. U1930402). We acknowledge the computational support from the Beijing Computational Science Research Center.

References

1 R. C. Zeller and R. O. Pohl, *Phys. Rev. B: Solid State*, 1971, **4**, 2029–2041.
2 M. P. Zaitlin and A. C. Anderson, *Phys. Rev. B: Solid State*, 1975, **12**, 4475–4486.
3 W. Schirmacher, T. Scopigno and G. Ruocco, *J. Non-Cryst. Solids*, 2015, **407**, 133–140.
4 W. Schirmacher, G. Ruocco and T. Scopigno, *Phys. Rev. Lett.*, 2007, **98**, 025501.
5 W. Schirmacher, B. Schmid, C. Tomaras, G. Baldi, G. Viliani, G. Ruocco and T. Scopigno, *Condens. Matter Phys.*, 2010, **13**, 23606.
6 W. Schirmacher, B. Schmid, C. Tomaras, G. Viliani, G. Baldi and G. Ruocco, *Phys. Status Solidi C*, 2008, **5**, 862–866.
7 W. Schirmacher, *Europhys. Lett.*, 2006, **73**, 892–898.
8 A. Marruzzo, W. Schirmacher, A. Fratalocchi and G. Ruocco, *Sci. Rep.*, 2013, **3**, 1407.
9 M. Wyart, *Europhys. Lett.*, 2010, **89**, 64001.
10 E. DeGiuli, A. Laversanne-Finot, G. Düring, E. Lerner and M. Wyart, *Soft Matter*, 2014, **10**, 5628–5644.
11 V. Vitelli, *Soft Matter*, 2010, **6**, 3007–3012.
12 T. S. Grigera, V. Martin-Mayor, G. Parisi, P. Urbani and P. Verrocchio, *J. Stat. Mech.: Theory Exp.*, 2011, **11**, P02015.
13 U. Buchenau, Yu. M. Galperin, V. L. Gurevich, D. A. Parshin, M. A. Ramos and H. R. Schober, *Phys. Rev. B: Condens. Matter Mater. Phys.*, 1992, **46**, 2798–2808.
14 G. Ruocco, F. Sette, R. Di Leonardo, D. Fioretto, M. Krisch, M. Lorenzen, C. Masciovecchio, G. Monaco, F. Pignon and T. Scopigno, *Phys. Rev. Lett.*, 1999, **83**, 5583–5586.
15 F. Sette, M. Krisch, C. Masciovecchio, G. Ruocco and G. Monaco, *Science*, 1998, **280**, 1550–1555.

This journal is © The Royal Society of Chemistry 2019

16 G. Ruocco and F. Sette, *J. Phys.: Condens. Matter*, 2001, **13**, 9141–9164.
17 C. Masciovecchio, A. Gessini, S. Di Fonzo, L. Comez, S. C. Santucci and D. Fioretto, *Phys. Rev. Lett.*, 2004, **92**, 247401.
18 P. Benassi, S. Caponi, R. Eramo, A. Fontana, A. Giugni, M. Nardone, M. Sampoli and G. Viliani, *Phys. Rev. B: Condens. Matter Mater. Phys.*, 2005, **71**, 1782201.
19 C. Masciovecchio, G. Baldi, S. Caponi, L. Comez, S. Di Fonzo, D. Fioretto, A. Fontana, A. Gessini, S. C. Santucci, F. Sette, G. Viliani, P. Vilmercati and G. Ruocco, *Phys. Rev. Lett.*, 2006, **97**, 035501.
20 A. Devos, M. Foret, S. Ayrinhac, P. Emery and B. Rufflé, *Phys. Rev. B: Condens. Matter Mater. Phys.*, 2008, **77**, 100201(R).
21 T. Scopigno, J.-B. Suck, R. Angelini, F. Albergamo and G. Ruocco, *Phys. Rev. Lett.*, 2006, **96**, 135501.
22 B. Rufflé, G. Guimbretière, E. Courtens, R. Vacher and G. Monaco, *Phys. Rev. Lett.*, 2006, **96**, 045502.
23 G. Monaco and V. M. Giordano, *Proc. Natl. Acad. Sci. U. S. A.*, 2009, **106**, 3659–3663.
24 G. Baldi, V. M. Giordano, G. Monaco and B. Ruta, *Phys. Rev. Lett.*, 2010, **104**, 195501.
25 G. Baldi, V. M. Giordano, B. Ruta, R. Dal Maschio, A. Fontana and G. Monaco, *Phys. Rev. Lett.*, 2014, **112**, 125502.
26 G. Baldi, M. Zanatta, E. Gilioli, V. Milman, K. Refson, B. Wehinger, B. Winkler, A. Fontana and G. Monaco, *Phys. Rev. Lett.*, 2013, **110**, 185503.
27 B. Ruta, G. Baldi, F. Scarponi, D. Fioretto, V. M. Giordano and G. Monaco, *J. Chem. Phys.*, 2012, **137**, 214502.
28 H. Mizuno, S. Mossa and J.-L. Barrat, *Proc. Natl. Acad. Sci. U. S. A.*, 2014, **111**, 11949–11954.
29 H. Mizuno and S. Mossa, 2019, arXiv:1906.08012.
30 S. Gelin, H. Tanaka and A. Lemaitre, *Nat. Mater.*, 2016, **15**, 1177–1181.
31 S. John and M. Stephen, *Phys. Rev. B: Condens. Matter Mater. Phys.*, 1983, **28**, 6358–6368.
32 H. Mizuno and A. Ikeda, *Phy. Rev. E*, 2018, **98**, 062612.
33 A. Moriel, G. Kapteijns, C. Rainone, J. Zylberg, E. Lerner and E. Bouchbinder, 2019, arXiv:1905.03378.
34 T. S. Grigera and G. Parisi, *Phys. Rev. E: Stat., Nonlinear, Soft Matter Phys.*, 2001, **63**, 045102(R).
35 L. Berthier, D. Coslovich, A. Ninarello and M. Ozawa, *Phys. Rev. Lett.*, 2016, **116**, 238002.
36 A. Ninarello, L. Berthier and D. Coslovich, *Phys. Rev. X*, 2017, **7**, 021039.
37 L. Wang, A. Ninarello, P. Guan, L. Berthier, G. Szamel and E. Flenner, *Nat. Commun.*, 2019, **10**, 26.
38 M. Ozawa, L. Berthier, G. Biroli, A. Rosso and G. Tarjus, *Proc. Natl. Acad. Sci. U. S. A.*, 2018, **115**, 6656.
39 E. Bitzek, P. Koskinen, F. Gähler, M. Moseler and P. Gumbsch, *Phys. Rev. Lett.*, 2006, **97**, 170201.
40 H. Staley, E. Flenner and G. Szamel, *J. Chem. Phys.*, 2016, **145**, 184505.
41 J. Helfferich, I. Lyubimov, D. Reid and J. J. de Pablo, *Soft Matter*, 2016, **12**, 5898.
42 I. Lyubimov, M. D. Ediger and J. J. de Pablo, *J. Chem. Phys.*, 2013, **139**, 144505.
43 S. Singh, M. D. Ediger and J. J. de Pablo, *Nat. Mater.*, 2013, **12**, 139.
44 X. Wang, W. Zheng, L. Wang and N. Xu, *Phys. Rev. Lett.*, 2015, **114**, 035502.
45 G. Monaco and S. Mossa, *Proc. Natl. Acad. Sci. U. S. A.*, 2009, **106**, 16097–16912.
46 E. A. A. Pogna, A. I. Chumakov, C. Ferrante, M. A. Ramos and T. Scopigno, *J. Phys. Chem. Lett.*, 2019, **10**, 427–432.
47 Y. Wang, L. Hong, Y. Wang, W. Schirmacher and J. Zhang, *Phys. Rev. B*, 2018, **98**, 174207.
48 Y. M. Beltukov, D. A. Parshin, V. M. Giordano and A. Tanguy, *Phys. Rev. E*, 2018, **98**, 023005.
49 N. Xu, V. Vitelli, M. Wyart, A. J. Liu and S. R. Nagel, *Phys. Rev. Lett.*, 2009, **102**, 038001.
50 V. Vitelli, N. Xu, M. Wyart, A. J. Liu and S. R. Nagel, *Phys. Rev. E: Stat., Nonlinear, Soft Matter Phys.*, 2010, **81**, 021301.
51 H. Shintani and H. Tanaka, *Nat. Mater.*, 2008, **7**, 870.
52 H. Mizuno, H. Shiba and A. Ikeda, *Proc. Natl. Acad. Sci. U. S. A.*, 2017, **114**, E9767–E9774.
53 P. G. Klemens, *Proc. – R. Soc. Edinburgh, Sect. A: Math. Phys. Sci.*, 1951, **208**, 108–133.
54 H. Mizuno, S. Mossa and J.-L. Barrat, *Phys. Rev. E: Stat., Nonlinear, Soft Matter Phys.*, 2013, **87**, 042306.
55 S. F. Swallen, K. L. Kearns, M. K. Mapes, Y. S. Kim, R. J. McMahon, M. D. Ediger, T. Wu, L. Yu and S. Satija, *Science*, 2007, **315**, 353–356.
56 E. A. A. Pogna, C. Rodríguez-Tinoco, G. Cerullo, C. Ferrante, J. Rodríguez-Viejo and T. Scopigno, *Proc. Natl. Acad. Sci. U. S. A.*, 2015, **112**, 2331–2336.
57 H. Mizuno, G. Ruocco and S. Mossa, arXiv:1905.10235.
58 E. Bouchbinder and E. Lerner, *New J. Phys.*, 2018, **20**, 073022.